Geosci. Model Dev. Discuss., 8, 2973–2990, 2015
www.geosci-model-dev-discuss.net/8/2973/2015/
doi:10.5194/gmdd-8-2973-2015

Geoscientific Model Development Discussions
Open Access

High resolution numerical modeling of mesoscale island wakes and sensitivity to static topographic relief data

C. G. Nunalee[1], **Á. Horváth**[2], **and S. Basu**[1]

[1]Department of Marine, Earth, and Atmospheric Sciences, North Carolina State University, Raleigh, NC, USA
[2]Leibniz Institute for Tropospheric Research, Leipzig, Germany

Received: 22 January 2015 – Accepted: 12 February 2015 – Published: 19 March 2015

Correspondence to: C. G. Nunalee (cgnunale@ncsu.edu)

Published by Copernicus Publications on behalf of the European Geosciences Union.

Abstract

Recent decades have witnessed a drastic increase in the fidelity of numerical weather prediction (NWP) modeling. Currently, both research-grade and operational NWP models regularly perform simulations with horizontal grid spacings as fine as 1 km. This migration towards higher resolution potentially improves NWP model solutions by increasing the resolvability of mesoscale processes and reducing dependency on empirical physics parameterizations. However, at the same time, the accuracy of high-resolution simulations, particularly in the atmospheric boundary layer (ABL), are also sensitive to orographic forcing which can have significant variability on the same spatial scale as, or smaller than, NWP model grids. Despite this sensitivity, many high resolution atmospheric simulations do not consider uncertainty with respect to selection of static terrain height dataset. In this paper, we use the Weather Research and Forecasting (WRF) model to simulate realistic cases of lower tropospheric flow over and downstream of mountainous islands using both the default global 30 s United States Geographic Survey terrain height dataset (GTOPO30) and the 3 s Shuttle Radar Topography Mission (SRTM) terrain height dataset. Our results demonstrate cases where the differences between GTOPO30-based and SRTM-based model terrain height are significant enough to produce entirely different orographic wake mechanics, such as vortex shedding vs. no vortex shedding. These results are also compared to MODIS visible satellite imagery and highlight the importance of considering uncertain static boundary conditions when running high-resolution mesoscale models.

1 Introduction

Massively-parallel computing platforms now enable regional-scale numerical weather prediction (NWP) models[1] to be easily integrated with fine-scale grid spacings, down

[1]In the context of this article, NWP models refer to models that may run in forecast or hindcast modes.

GMDD
8, 2973–2990, 2015

to approximately 1 km horizontally. A valuable benefit of such high-resolution models is their capability to simulate orographically induced flow phenomena. Examples of such phenomena include gap-winds (Mass et al., 2014), lee-rotors (Ágústsson and Ólafsson, 2014), and wake vortices (Li et al., 2008). The accuracy of model simulations of orographic flows has been verified against a suite of observational data including, but not limited to, ground-based instruments e.g., lidar (Lesouëf et al., 2013), mesonets (Bieringer et al., 2013); satellite-based remote sensing instruments e.g., SAR (Miglietta et al., 2013); and airborne measurement platforms e.g., aircraft (Gioli et al., 2014), radiosonde (Nunalee and Basu, 2014). Despite the increased resolvability, and overall fidelity, offered by finer resolution models as it pertains to orographic flows, mesoscale NWP models are still constrained by multiple factors (Doyle et al., 2013) such as necessary physics parameterizations (Draxl et al., 2014). The treatment of sub-grid scale (i.e., sub-mesoscale) processes such as turbulence, radiative transfer, moisture phase change, etc. collectively contributes to the uncertainty of model solutions (see Coiffier, 2011). At the same time, it has also been demonstrated that model uncertainty can be increased through the prescription of inaccurate, or unrepresentative, time-dependent atmospheric boundary conditions (Kumar et al., 2011; Pielke Sr., 2013). In the past decade, advanced data assimilation techniques, coupled with improved remote sensing capabilities, have been shown to reduce simulation uncertainty (Ancell et al., 2011; Bieringer et al., 2013) and increase forecast skill (Pu et al., 2013). While great efforts have been expended to identify sources of NWP error with respect to model configuration (i.e., physics parameterizations) and dynamic (meteorological) boundary conditions, often overlooked is the sensitivity of model solutions to static boundary conditions, namely topographic relief.

Presently, there exists several global terrain height datasets which can be used by regional-scale NWP models. One of the most used surface relief datasets, named GTOPO30, was developed by the United States Geographic Survey and comprised through a synthesis of numerous international digital elevation models. GTOPO30 contains maximum spatial resolution of 30 arc seconds and is the default dataset for many community models such as the Weather Research and Forecasting (WRF) model. Aside from GTOPO30 data, other satellite-derived global terrain height datasets also exist such as the Shuttle Radar Topography Mission (SRTM) (Farr et al., 2007), and the Advanced Spaceborne Thermal Emission and Reflection Radiometer (ASTER) (Abrams et al., 2002). These datasets offer higher spatial resolutions globally of 3 arc seconds and 1 arc second, respectively. The construction of surface terrain height grids in NWP models from source datasets, such as GTOPO30 or SRTM, typically involves sub-grid scale averaging of the source data, grid-scale spatial interpolation during data ingestion, and/or preprocessing smoothing effects (e.g., see the WRF model Preprocessing System Documentation; NCAR, 2014). Although in many circumstances these activities are necessary, they can effectively result in under-resolved topographic relief. Under-resolved terrain height implies that the NWP model generated terrain height does not fully capture the relevant features of the natural topography described by the source data (Jiménez and Dudhia, 2012) and can result in terrain height discrepancies on the order of tens to hundreds of meters (Jiménez and Dudhia, 2013). Such discrepancies have been shown to result in significant error in simulated low-level wind fields (Rife and Davis, 2005; Jiménez et al., 2010; Santos-Alamillos et al., 2013). Aside from under-resolved terrain height in modeled grids, which is essentially an oversimplification of the source terrain height data, we show in this paper that uncertainty in source terrain height datasets themselves can be significant enough to result in fundamental differences in simulated orographic flow mechanics. This result illustrates that the sensitivity of NWP models can be more complex than 1st-order biases recently documented by Teixeira et al. (2014).

In this paper, we simulate two realistic cases of atmospheric flow past mountainous islands; for each case, we run the WRF model simulations using GTOPO30 and SRTM source terrain height data while keeping all other model configurations identical. From the results, we comment on the fundamental differences in simulated atmospheric wake patterns associated with the two terrain height fields. At the same time we compare the simulated flow features to those expected from visible satellite imagery.

GMDD
8, 2973–2990, 2015

Our results will demonstrate that selection of terrain height source data can, in some cases, be critical to successfully capturing the fundamental mechanics of mesoscale orographic wakes.

2 Case studies and modeling details

Two historical atmospheric events were considered in this paper, both corresponding to cases of flow past mountainous islands. Since the islands were far from any upstream surface heterogeneity, only the local terrain features associated with the islands acted to perturb the local winds and consequent cloud structures. For these events, the wind wake characteristics associated with each island were indicated by distinct cloud structures captured by visible satellite imagery provided by the Moderate Resolution Imaging Spectroradiometer (MODIS) instrument. The modeled wind wake patterns of the events were compared to one another and the differences were documented in the context of the inferred wake patterns shown in satellite imagery.

The first, and primary, case study involved the Spanish island of Gran Canaria (GC) off the west coast of Northern Africa on 30 April 2007. MODIS visible satellite imagery from this day (Fig. 1a) revealed a coherent pattern of dipole vortices (i.e., von Kármán vortices) being shed downstream of GC around 10:30 UTC. GC has a diameter of approximately 50 km at sea level and has a peak elevation of 1948 m m.s.l. GC's SRTM-based topography is shown in Fig. 1 for reference.

The second case study presented here involves flow past several islands which collectively comprise the Lesser Antilles (LA) in the Eastern Caribbean. On 31 July 2013, MODIS visible satellite imagery of the Lesser Antilles region (Fig. 1c) illustrated distinct wakes behind all of the major islands of the LA. Contrary to the GC case which had a coherent vortex shedding wake regime, the LA case had weak wind wakes where the rotation behind each island was not strong enough to counter the background wind flow. Furthermore, the wakes were correlated with a reduction in cumulus cloudiness and darker sea surface color, a phenomenon investigated by Smith et al. (1997). The

GMDD
8, 2973–2990, 2015

windward islands of the LA are generally lower than GC but, nonetheless, are predominately mountainous with peak elevations near 1 km for each island (see Table in Fig. 1d).

The numerical simulations performed in this study used the Weather Research and Forecasting (WRF) model which was initialized by ERA-Interim reanalysis data (physics configurations are shown in Table 1). The simulations used a nested four domain configuration centered on the islands of interest. Of note, a horizontal grid spacing of 1 km was chosen in the inner-most domain (d04) while the parent domains (d03–d01) used grid spacings of 3, 9, and 27 km, respectively. Additionally, in d04 the control simulations used GTOPO30 terrain height while the experimental simulations used terrain height data interpolated from SRTM 3 arc second data. d01, d02, and d03 used 10, 5, and 2 min GTOPO30 terrain height, respectively. All other modeling variables were held constant between the control simulations and experimental simulations. For both the original GTOPO30 and SRTM terrain height fields, the default smoothing and interpolation methods were selected. That is, 1 pass of the built-in WRF Preprocessing System (WPS) smoother-desmoother and 4 point averaging interpolation, respectively.

3 Gran Canaria case study

In this section, we analyze the atmospheric flow patterns downstream of GC as simulated by the WRF model with GTOPO30 terrain and SRTM terrain. Before beginning the analysis, we compare the discrepancies between the two terrain height data fields. Figure 2 presents a southern view of the model terrain height for GC as generated by GTOPO30 and SRTM. Notice that aside from increased ruggedness in the SRTM-based terrain height, there is also a significant increase in peak terrain height of GC island of nearly 1 km. Additionally, Fig. 2 also illustrates the upstream mean potential temperature cross-section in the lower troposphere on the day of 30 April 2007. Within the potential temperature cross-section, a well-mixed planetary boundary layer (PBL) can be identified by the nearly constant potential temperature in the lowest 800 m of

GMDD
8, 2973–2990, 2015

the atmosphere. Above this layer, in the free atmosphere, a thermal capping inversion was present. Most importantly for the purposes of this paper, is that the increase in peak elevation of GC with the SRTM data makes the modeled GC island penetrate into the stably stratified free atmosphere.

As the original GTOPO30-based elevation of GC was predominately within the well mixed PBL, the simulated flow around it was mostly 3 dimensional. That is, the impinging air parcels were able to rise and cross the crest of the island barrier and then descend on the lee slope without significant buoyant restriction. This effect acted to produce the unorganized wake pattern shown in the lower-left panel of Fig. 2. Alternatively, with the SRTM-based elevation, the increased topographic steepness along with the layer of stable stratification beneath the maximum height of the island caused much of the flow to split and pass around the lateral flanks of GC. This flow behavior generated coherent lee vortices (i.e., von Kámán vortices) which were shed downstream of the island, similar to what was observed by the MODIS satellite imagery shown in Fig. 1.

In addition to invoking differences in the simulated wake pattern of GC, the SRTM-based and GTOPO30-based simulations also produced substantial variability to the wind regime on GC itself. In Fig. 3, an instantaneous streamwise wind speed cross section is presented for both simulations. Of particular note is the wind speed extrema (greater than $17\,\mathrm{m\,s^{-1}}$) on the crest of GC in the GTOPO30-based simulation. This zone of high wind speed was a result of the Venturi effect caused by compression of the air column as it passed over the crest of the island. Alternatively, in the SRTM-based simulation this zone of strong wind speed was not simulated due to the lack of significant air column compression over GC. Instead, the lateral flow around GC produces a zone of weak wind speed along the island centerline with respect to the flow direction.

GMDD
8, 2973–2990, 2015

4 Lesser Antilles case study

The second case study presented here deals with boundary layer flow impinging on the Eastern slopes of the Lesser Antilles (LA) island archipelago. As can be seen in Fig. 1, the wake signatures from all of the major islands in this region persisted for up to approximately 300 km downstream. Contrary to the GC case, the wake patterns in the LA case did not contain strong enough vorticity to counter the ambient wind speed and therefore coherent wake vortices did not form. This type of wake pattern has been called a weak wake pattern by Smith et al. (1997), and forms in conditions of slower wind speed and lower island height in comparison with the vortex shedding patterns with the GC case.

In the upper panels of Fig. 4, the regional topographic relief is shown for the GTOPO30-based simulation vs. the SRTM-based simulation. Of particular note is the fact that the island of Dominica, one of the more prominent of the islands in the LA in the SRTM-based simulation, is represented as flat (1 m m.s.l.) in the the GTOPO30-based model elevation. At the same time, other neighboring islands (e.g., St. Vincent) appear relatively similar, despite them being slightly smaller in size in the GTOPO30-based model. The differences in the depiction of Dominica's relief in the two simulations manifested in substantial differences in regards to the simulated 6 h mean surface wind speeds. The lower panels in Fig. 4 show the mean surface wind fields simulated by the two model runs. Most notably, the weak wind wake associated with Dominica is nearly non-existent in the GTOPO30-based simulation while it extends hundreds of km in the SRTM based simulation. In addition, the zone of enhanced wind speed associated with funneling between Dominica and its northern neighbor of Guadeloupe is increased in the SRTM-based simulation. Lastly, the unique shapes of the individual island wakes showed signs of variability between the GTOPO30 and SRTM based simulations.

GMDD
8, 2973–2990, 2015

5 Conclusions

In this work, we have simulated two realistic cases of atmospheric flow past mountainous islands using the WRF model. For each case, we explored the sensitivity of the simulated wake patterns with respect to two different terrain height source datasets (i.e., GTOPO30 and SRTM). Our results show cases where the differences in modeled terrain height corresponded to fundamental differences in simulated wake mechanics. For the GC case, the simulation which used GTOPO30 terrain height had a peak island elevation which was nearly 1 km lower than that in the SRTM-based simulation. For this case, the GTOPO30-based terrain did not reach the stably stratified thermal inversion above the planetary boundary layer while the SRTM-based terrain extended hundreds of meters into the free atmosphere. This difference resulted in substantially less vertical vorticity downstream of GC island, along with an area of wind speed extrema on the crest of the island in the GTOPO30-based simulation. In other words, the SRTM-based simulation produced more significant lateral flow around the island and downstream von Kármán vortices, in agreement with MODIS visible satellite imagery, while the GTOPO30-based simulation facilitated anomalous Venturi-type wind speed-up on the crest of the island and incoherent downstream vortices.

For the LA case, the GTOPO30-based model terrain represented the island of Dominica to be essentially flat and near sea level (i.e., 1 m m.s.l.) and consequently resulted in no surface wind wake pattern. At the same time, the SRTM-based simulation resulted in a weak wind wake field which extended hundreds of km downstream of Dominica. The latter was similar to what was illustrated in visible satellite imagery.

This work explored the value of using representative terrain height source data for high resolution mesoscale modeling activities. Moreover, it was highlighted that considerable care should be taken while selecting orographic relief input data when simulating atmospheric flow over, around, and downstream of remote mountainous islands (e.g., Gran Canaria and Dominica). That being said, future studies should evaluate the

GMDD
8, 2973–2990, 2015

accuracy of global terrain datasets for other locations and their representativeness for mesoscale modeling.

Acknowledgements. The authors acknowledge computational and financial support received from the Renaissance Computing Institute in addition to financial support received from the Department of Defense AFOSR under award number (FA9550-12-1-0449). Any opinions, findings and conclusions or recommendations expressed in this material are those of the authors and do not necessarily reflect the views of the Department of Defense.

References

Abrams, M., Hook, S., and Ramachandran, B.: ASTER User Handbook Version 2, Tech. rep., NASA – Jet Propulsion Laboratory, 4800, 2002. 2976

Ágústsson, H. and Ólafsson, H.: Simulations of observed lee waves and rotor turbulence, Mon. Weather Rev., 142, 832–849, 2014. 2975

Ancell, B. C., Mass, C. F., and Hakim, G. J.: Evaluation of surface analyses and forecasts with a multiscale ensemble Kalman filter in regions of complex terrain, Mon. Weather Rev., 139, 2008–2024, 2011. 2975

Bieringer, P. E., Ray, P. S., and Annunzio, A. J.: The effect of topographic variability on initial condition sensitivity of low-level wind forecasts. Part II: Experiments using real terrain and observations, Mon. Weather Rev., 141, 2156–2172, 2013. 2975

Chen, F. and Dudhia, J.: Coupling an advanced land-surface/hydrology model with the Penn State/NCAR MM5 modeling system, Mon. Weather Rev., 129, 587–604, 2001. 2986

Coiffier, J.: Fundamentals of Numerical Weather Prediction, Cambridge University Press, 2011. 2975

Doyle, J. D., Epifanio, C. C., Persson, A., Reinecke, P. A., and Zängl, G.: Mesoscale modeling over complex terrain: numerical and predictability perspectives, in: Mountain Weather Research and Forecasting, Springer, 531–589, 2013. 2975

Draxl, C., Hahmann, A. N., Peña, A., and Giebel, G.: Evaluating winds and vertical wind shear from Weather Research and Forecasting model forecasts using seven planetary boundary layer schemes, Wind Energy, 17, 39–55, 2014. 2975

Dudhia, J.: Numerical study of convection observed during the winter monsoon experiment using a mesoscale two-dimensional model, J. Atmos. Sci., 46, 3077–3107, 1989. 2986

Farr, T. G., Rosen, P. A., Caro, E., Crippen, R., Duren, R., Hensley, S., Kobrick, M., Paller, M., Rodriguez, E., Roth, L., Seal, D., Shaffer, S., Shimada, J., Umland, J., Werner, M., Oskin, M., Burbank, D., and Alsdorf D.: The shuttle radar topography mission, Rev. Geophys., 45, RG2004, doi:10.1029/2005RG000183, 2007. 2976

Gioli, B., Gualtieri, G., Busillo, C., Calastrini, F., Gozzini, B., and Miglietta, F.: Aircraft wind measurements to assess a coupled WRF-CALMET mesoscale system, Meteorol. Appl., 21, 117–128, 2014. 2975

Hong, S.-Y., Dudhia, J., and Chen, S.-H.: A revised approach to ice microphysical processes for the bulk parameterization of clouds and precipitation, Mon. Weather Rev., 132, 103–120, 2004. 2986

Janjić, Z. I.: The step-mountain ETA coordinate model: further developments of the convection, viscous sublayer, and turbulence closure schemes, Mon. Weather Rev., 122, 927–945, 1994. 2986

Jiménez, P. A. and Dudhia, J.: Improving the representation of resolved and unresolved topographic effects on surface wind in the WRF model, J. Appl. Meteorol. Clim., 51, 300–316, 2012. 2976

Jiménez, P. A. and Dudhia, J.: On the ability of the WRF model to reproduce the surface wind direction over complex terrain, J. Appl. Meteorol. Clim., 52, 1610–1617, 2013. 2976

Jiménez, P. A., González-Rouco, J. F., García-Bustamante, E., Navarro, J., Montávez, J. P., de Arellano, J. V.-G., Dudhia, J., and Muñoz-Roldan, A.: Surface wind regionalization over complex terrain: evaluation and analysis of a high-resolution WRF simulation, J. Appl. Meteorol. Clim., 49, 268–287, 2010. 2976

Kain, J.: The Kain–Fritsch convective parameterization: an update, J. Appl. Meteorol., 43, 170–181, 2004. 2986

Kumar, A., Done, J., Dudhia, J., and Niyogi, D.: Simulations of Cyclone Sidr in the Bay of Bengal with a high-resolution model: sensitivity to large-scale boundary forcing, Meteorol. Atmos. Phys., 114, 123–137, 2011. 2975

Lesouëf, D., Gheusi, F., Chazette, P., Delmas, R., and Sanak, J.: Low tropospheric layers over Reunion Island in lidar-derived observations and a high-resolution model, Bound.-Layer Meteorol., 149, 425–453, 2013. 2975

Li, X., Zheng, W., Zou, C., and Pichel, W.: A SAR observation and numerical study on ocean surface imprints of atmospheric vortex streets, Sensors, 8, 3321–3334, 2008. 2975

Mass, C. F., Warner, M. D., and Steed, R.: Strong westerly wind events in the Strait of Juan de Fuca, Weather Forecast., 29, 445–465, 2014. 2975

Miglietta, M. M., Zecchetto, S., and De Biasio, F.: A comparison of WRF model simulations with SAR wind data in two case studies of orographic lee waves over the Eastern Mediterranean Sea, Atmos. Res., 120, 127–146, 2013. 2975

Mlawer, E., Taubman, S., Brown, P., Iacono, M., and Clough, S.: Radiative transfer for inhomogeneous atmosphere: RRTM, a validated correlated-k model for the longwave, J. Geophys. Res., 102, 16663–16682, 1997. 2986

Monin, A. and Obukhov, A.: Basic laws of turbulent mixing in the surface layer of the atmosphere, Contrib. Geophys. Inst. Acad. Sci. USSR, 151, 163–187, 1954. 2986

NCAR: User's Guide for Advanced Research WRF Modeling System: CH3, The WRF Preprocessing System, available at: http://www2.mmm.ucar.edu/wrf/users/docs/user_guide_V3/users_guide_chap3.htm (last access: 15 April 2014), 2014. 2976

Nunalee, C. G. and Basu, S.: Mesoscale modeling of coastal low-level jets: implications for offshore wind resource estimation, Wind Energy, 17, 1199–1216, 2014. 2975

Pielke Sr., R. A.: Mesoscale Meteorological Modeling, Vol. 98, Academic Press, Waltham, MA, USA Oxford, UK Amsterdam, the Netherlands, available at: http://books.google.com/books?hl=en&lr=&id=ExlFulltapcC&oi=fnd&pg=PR1&dq=mesoscale+meteorological+modeling+pielke (last access: 17 March 2015), 2013. 2975

Pu, Z., Zhang, H., and Anderson, J.: Ensemble Kalman filter assimilation of near-surface observations over complex terrain: comparison with 3DVAR for short-range forecasts, Tellus A, 65, 19620, doi:10.3402/tellusa.v65i0.19620, 2013. 2975

Rife, D. L. and Davis, C. A.: Verification of temporal variations in mesoscale numerical wind forecasts, Mon. Weather Rev., 133, 3368–3381, 2005. 2976

Santos-Alamillos, F., Pozo-Vázquez, D., Ruiz-Arias, J., Lara-Fanego, V., and Tovar-Pescador, J.: Analysis of WRF model wind estimate sensitivity to physics parameterization choice and terrain representation in Andalusia (Southern Spain), J. Appl. Meteorol. Clim., 52, 1592–1609, 2013. 2976

Smith, R. B., Gleason, A. C., Gluhosky, P. A., and Grubišic, V.: The wake of St. Vincent, J. Atmos. Sci., 54, 606–623, 1997. 2977, 2980

Teixeira, J. C., Carvalho, A. C., Carvalho, M. J., Luna, T., and Rocha, A.: Sensitivity of the WRF model to the lower boundary in an extreme precipitation event – Madeira island case study, Nat. Hazards Earth Syst. Sci., 14, 2009–2025, doi:10.5194/nhess-14-2009-2014, 2014. 2976

Table 1. Model physics configurations.

Parameterization	Name	Reference
Microphysics	WRF Single-Moment 5-class	Hong et al. (2004)
Longwave Radiation	RRTM Longwave	Mlawer et al. (1997)
Shortwave Radiation	Dudhia Shortwave Radiation	Dudhia (1989)
Convection	Kain–Fritsch (d01 and d02)	Kain (2004)
Land Surface	Noah Land Surface Model	Chen and Dudhia (2001)
Planetary Boundary Layer	Mellor–Yamada–Janjić	Janjić (1994)
Surface Layer	Monin–Obukhov Similarity Theory	Monin and Obukhov (1954)

GMDD
8, 2973–2990, 2015

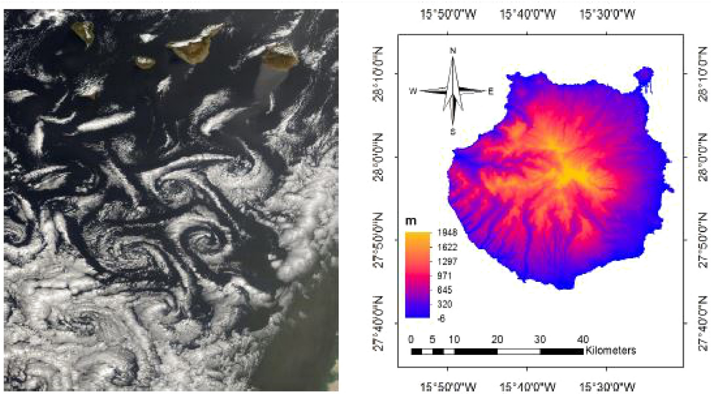

(a) (b)

(c)

Symbol	Island	Peak Elevation
A	Guadeloupe	1467 m
B	Dominica	1447 m
C	Martinique	1397 m
D	St. Lucia	950 m
E	St. Vincent	1234 m
F	Grenada	840 m

(d)

Figure 1. MODIS-TERRA visible satellite imagery of the Canary Islands on 30 April 2007 with Gran Canaria in the upper left **(a)** and SRTM terrain height profile of Gran Canaria **(b)**. MODIS-TERRA image of the Lesser Antilles on 1 August 2013 **(c)**. SRTM-derived peak elevation for each of the major windward islands in the Lesser Antilles **(d)**.

GMDD
8, 2973–2990, 2015

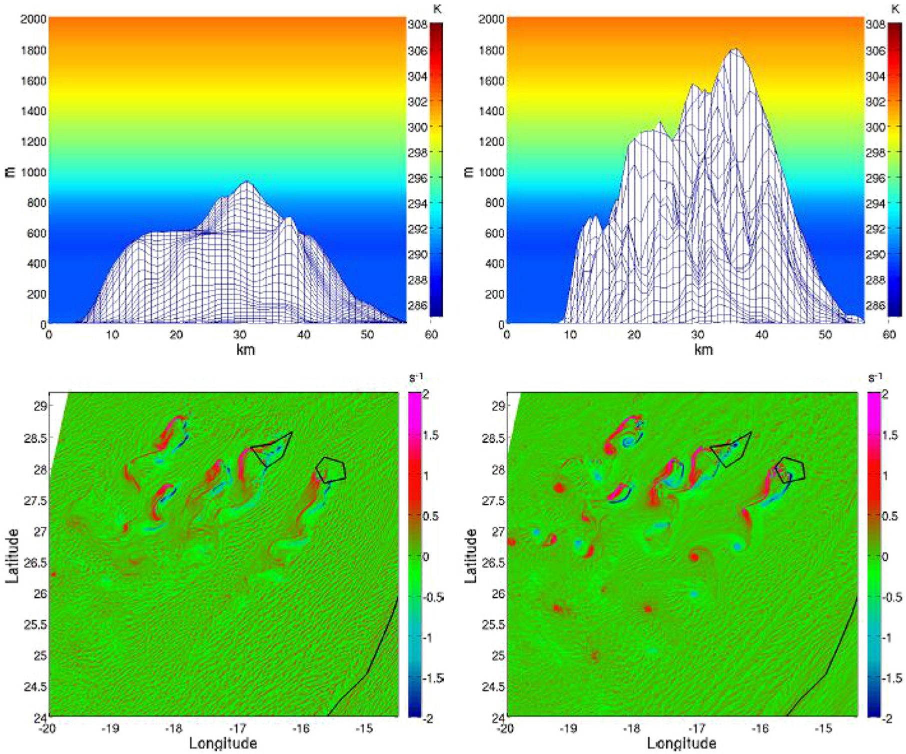

Figure 2. The WRF model's default 30 s USGS terrain height (upper left) and interpolated SRTM terrain height (upper right) of Gran Canaria as viewed from due South. Background color-scheme represents ambient upstream potential temperature profile. Lower left and right panels depict instantaneous relative vertical vorticity integrated vertically across the lowest 15 grid levels for the GTOPO30-based and SRTM-based simulations, respectively.

GMDD
8, 2973–2990, 2015

Title Page
Abstract | Introduction
Conclusions | References
Tables | Figures
◂◂ | ▸▸
◂ | ▸
Back | Close
Full Screen / Esc
Printer-friendly Version
Interactive Discussion

GMDD

8, 2973–2990, 2015

High resolution numerical modeling of mesoscale island wakes

C. G. Nunalee et al.

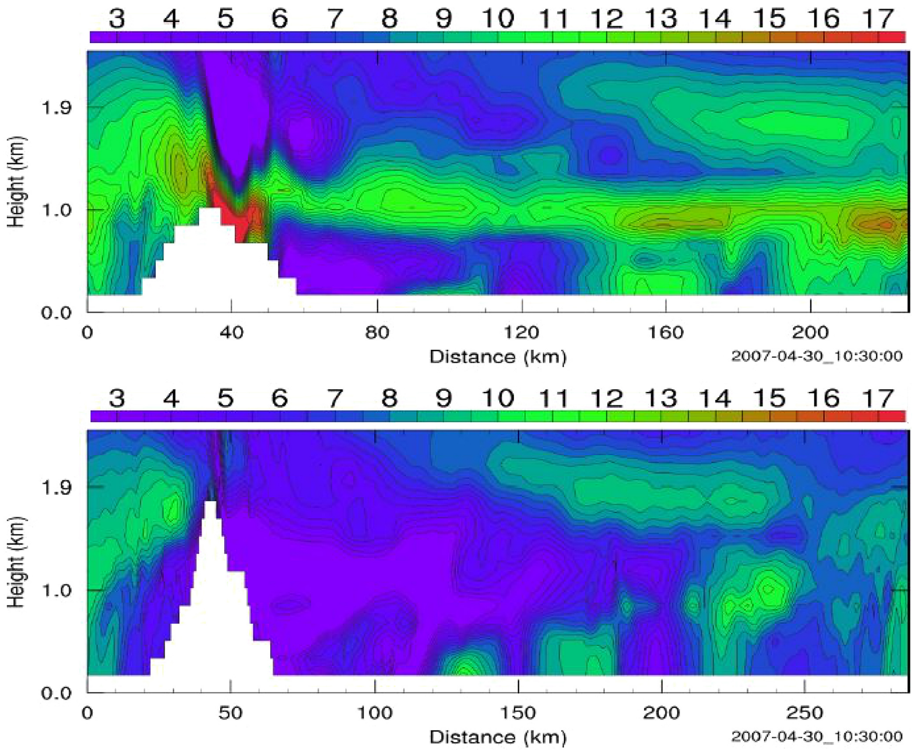

Figure 3. Instantaneous wind speed cross-sections for the GTOPO30-based (top panel) and SRTM-based (bottom panel) simulations at 10:30 UTC on 30 April 2007. Cross sections are oriented in the streamwise axis with inflow to the left.

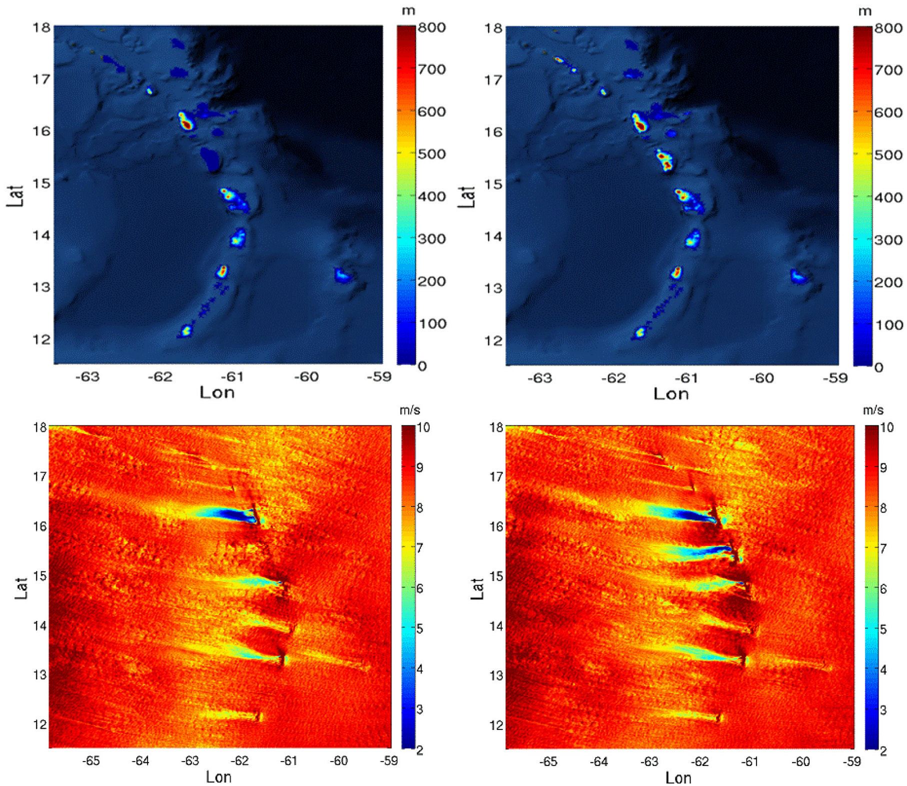

Figure 4. The WRF model's GTOPO30-based terrain height (upper left) and interpolated SRTM terrain height (upper right). Lower left and right panels depict averaged wind speed in the boundary layer from 06:00–12:00 UTC as simulated by the GTOPO30-based run and SRTM-based run, respectively.

GMDD
8, 2973–2990, 2015

High resolution numerical modeling of mesoscale island wakes

C. G. Nunalee et al.

Title Page
Abstract | Introduction
Conclusions | References
Tables | Figures
◀I | ▶I
◀ | ▶
Back | Close
Full Screen / Esc
Printer-friendly Version
Interactive Discussion